Proceedings of the 6th International Conference on the Application of Physical Modelling in Coastal and Port Engineering and Science (Coastlab16)

Ottawa, Canada, May 10-13, 2016

EXPERIMENTAL MODELLING OF MACRO-ROUGHNESS EFFECTS ON TSUNAMI-INDUCED PRESSURE IN IDEALIZED URBAN ENVIRONMENTS

TORI TOMICZEK[1], ADI PRASETYO[2], NOBUHITO MORI[2], TOMOHIRO YASUDA[2], ANDREW KENNEDY[1]

1 University of Notre Dame, USA, vtomicze@nd.edu, Andrew.B.Kennedy.117@nd.edu

2 Kyoto University, Japan, madjutakgentar@yahoo.com, mori.nobuhito.8a@kyoto-u.ac.jp, tomo@oceanwave.jp

ABSTRACT

Wave experiments were conducted on a 1:20 length scale at the Hybrid Tsunami Flume in Ujigawa (HyTOFU) to measure the pressure, velocity and water surface elevation on and around structural elements. Many design equations use bare-earth water surface elevations to predict design tsunami pressures; therefore, we compared the maximum water surface elevations of waves propagating across a bare beach to the water surface profiles recorded in front of an experimental obstacle. Adding structural elements to represent urban macro-roughness obstacles significantly changed the water profile for broken waves. For trials in which waves propagated across the beach as turbulent bores, the water surface elevation measured in front of a structure was between 4.5 and 7 times as large as the water surface elevation measured without urban roughness elements, depending on the horizontal location of the structure from shore. Design equations that recommend bare-earth water surface elevations to estimate tsunami-induced pressures were evaluated, and estimated values were compared with peak pressures recorded by gauges positioned on the structural element. Results indicated good agreement for nonbreaking waves but underestimation of peak pressures for breaking waves. Consideration of the water profile including wave-structure interaction yielded better agreement between predicted and measured pressures.

KEYWORDS: tsunami design, macro-roughness effects, pressure impulse, slamming coefficient.

INTRODUCTION

Tsunamis pose significant threats to coastal communities worldwide: recent tsunamis that have caused significant damage in coastal regions include the Indian Ocean Tsunami (2004), the South Pacific Tsunami (2009), and the Tohoku Earthquake Tsunami (2011). The Indian Ocean Tsunami on 26 December, 2004, generated waves up to 30 m high that left over 230,000 people dead or missing and caused extensive damage in countries bordering the Indian Ocean (e.g. Dalrymple and Kriebel, 2005, Papadopoulos et al., 2006, Tsuji et al., 2006, Koshimura et al., 2009, Leone et al., 2011). The South Pacific Tsunami of 29 September 2009 and the Chilean Tsunami of 27 February 2010 also caused substantial damage and loss of life in local villages (e.g. Reese et al., 2011, Mas et al., 2012). On 11 March 2011, the Tohoku Earthquake Tsunami caused severe damage to over 400,000 homes and catastrophic loss of life along the east coast of Japan (e.g. Mimura et al., 2011, Mori et al., 2011, Udo et al., 2012, Suppasri et al., 2013). The magnitude and extent of damage was surprising given Japan's extensive history of tsunamis, which led to the country's development of sophisticated tsunami countermeasures and warning systems (Zaré and Afrouz, 2012). Therefore, local and national governments across the globe must evaluate their tsunami response and preparedness plans to protect citizens, defend structures from damage, and ensure the safety and vitality of coastal communities.

Post disaster field surveys have been useful in evaluating the design and construction of tsunami mitigation structures in their ability to withstand a tsunami and prevent damage to local communities. However, it is difficult to estimate many hydrodynamic conditions from survey data; therefore, many reconnaissance-based fragility functions derived from damage surveys assume that the entire tsunami-induced load is based on the maximum water depth (Reese et al., 2011, Mas et al., 2012, Suppasri et al., 2013). Numerical simulations such as COULWAVE (Lynett et al., 2002), and NHWAVE (Ma et al., 2012) have simulated tsunami events over real topographies and given useful estimates of inundation, runup, and current velocities. Recent fragility models have included results from such numerical simulations to relate structural vulnerability to local hydrodynamic conditions (e.g. Suppasri et al., 2011). However, wave-structure interaction is difficult to model (Petukhin, et al., 2012), and many phase resolving models remove buildings and the related macro-roughness effects on wave

transformation in order to allow for efficient calculations (e.g. Westerink et al., 2008, Parsons et al., 2014, Grilli et al., 2015, Zhang et al., 2014). A more thorough understanding of wave propagation through urban environments will enhance the validity and robustness numerical simulations.

In addition to numerical models, laboratory experiments provide valuable datasets of tsunami propagation. Recent physical models have measured tsunami-induced water surface elevations, velocities, and pressures on and around structures and on scale models of cities; other experiments have tested the reliability of tsunami protection structures (e.g. Fujima et al., 2009, Bradner et al., 2009, Hsiao and Lin, 2010, Thomas and Cox, 2012, Park et al., 2013). However, many previous experiments have considered idealized tsunami profiles; real tsunami events have shown complex water surface profiles that involve both slow and quick water level increases (Fujima et al., 2009, Kawai et al., 2012, Goseberg et al., 2013). Likewise, waves breaking on structures are associated with complex turbulent and nonlinear effects; this turbulent impact can cause impulsive forces that generate debris and may cause significant structural damage. Laboratory measurements of tsunami-induced pressures have recorded very large, short-duration pressure peaks corresponding with wave impact and a following quasi-hydrostatic pressure (e.g. Fujima et al., 2009, Bradner et al., 2009, Thomas and Cox, 2012). Although Bradner et al. (2009) found that for large-inertia structures the impulse pressure may not translate to a slamming force, these pressures must not be neglected for non-engineered structures or when considering localized or debris-generating damage. However, it is difficult to relate wave conditions to expected peak pressures: previous experiments have noted that identical wave conditions have shown large variations in measured peak pressures (Chen and Melville, 1998). The energy transferred when a wave impacts a vertical structure causes splash effects that may be observed as a water jet accelerating vertically up the wall (Cooker and Peregrine 1995). This splashing can increase inundation and damage in nearshore communities during a tsunami.

As physical and numerical simulations of wave-structure interaction continue to improve, engineers, city planners, and governmental agencies use existing historical damage data, numerical simulations, and laboratory experiments to provide tsunami mitigation practices for communities located in vulnerable regions. These practices include developing sophisticated tsunami warning and evacuation systems for community residents as well as publishing conservative tsunami design equations for structural resilience. For example, both the American Society of Civil Engineers (ASCE) and the Japanese Cabinet Office (JCO) provide methods to estimate the maximum pressure caused by a tsunami. The equations provided by the ASCE and JCO calculate tsunami-induced loads based on the maximum tsunami inundation depth, h_{max}. This depth is an important consideration in tsunami design; however, due to the complexity of recent tsunami profiles and the processes associated with the interaction of the tsunami wave with a coastal structure, inputs into design equations are subject to error. Tsunamis propagate shoreward as a turbulent bore, a gradual rise and fall of the water level, or as a breaking wave; the Tohoku Earthquake Tsunami of 2011 was characterized by leading short, peaky waves with a long tail (Yeh, et al., 2009, Kawaii et al., 2012). Furthermore, the onshore propagation of waves will be affected by local topographies, structures, and tsunami countermeasures, termed macro-roughness elements (Irish et al., 2014, Thomas, et al., 2015). Design equations must make simplifying assumptions in order to be applicable to a wide range of coastal developments and wave characteristics; both the ASCE (2015) and JCO (2005) equations assume that h_{max} is the maximum depth at the structure's location with no obstacle affecting tsunami propagation. We analyzed the effects of macro-roughness elements on changing the water surface profile and peak pressure of waves with varied offshore characteristics through a series of experiments conducted at Kyoto University's Hybrid Tsunami Open Flume in Ujigawa (HyTOFU). Using experimental data, we compared the onshore water surface profiles recorded on a bare beach and with the addition of a structural obstacle, and we compared pressures predicted by design equations to peak pressures measured by pressure gauges mounted on an experimental specimen.

DESIGN STANDARDS

The design equation proposed by the JCO (2005) is based on laboratory measurements performed by Asakura et al. (2000) on 2d scale models. From these experiments, Asakura et al. (2000) developed an empirical relation that estimated the tsunami pressure as a triangular distribution with base pressure p_{max} equal to three times the hydrostatic pressure (see Figure 1a); that is,

$$p_{\max} = 3\rho g h_{\max}, \tag{1}$$

where ρ and g are the density of water and the acceleration due to gravity, respectively. In Equation (1), h_{max} is taken as the height of the bore at the structure, without considering splash or other phenomena associated with wave-structure interaction. Using this pressure, the maximum force may then be estimated by applying the triangular distribution over a height ($3h_{max}$). This equation has been examined by multiple studies; for example, Nakano (2008) observed damage after the Indian Ocean Tsunami and calculated a coefficient, α, for damaged homes by assuming the tsunami pressure was equal to the lateral resistance of the structure at elevation z above ground level:

$$p'_{\max} = \rho g(\alpha h_{\max} - z) \tag{2}$$

Nakano (2008) found that the coefficient α=3 was reasonably able to distinguish between damaged and surviving structures, but debris and other environmental factors may make the equation less conservative. Similar evaluations of Equation (1) have been performed experimentally (e.g. Fujima et al., 2009, Achmed, et al., 2009), and alternative coefficients have been suggested; however, Equation (1) remains the standard for tsunami-resistant design in Japan.

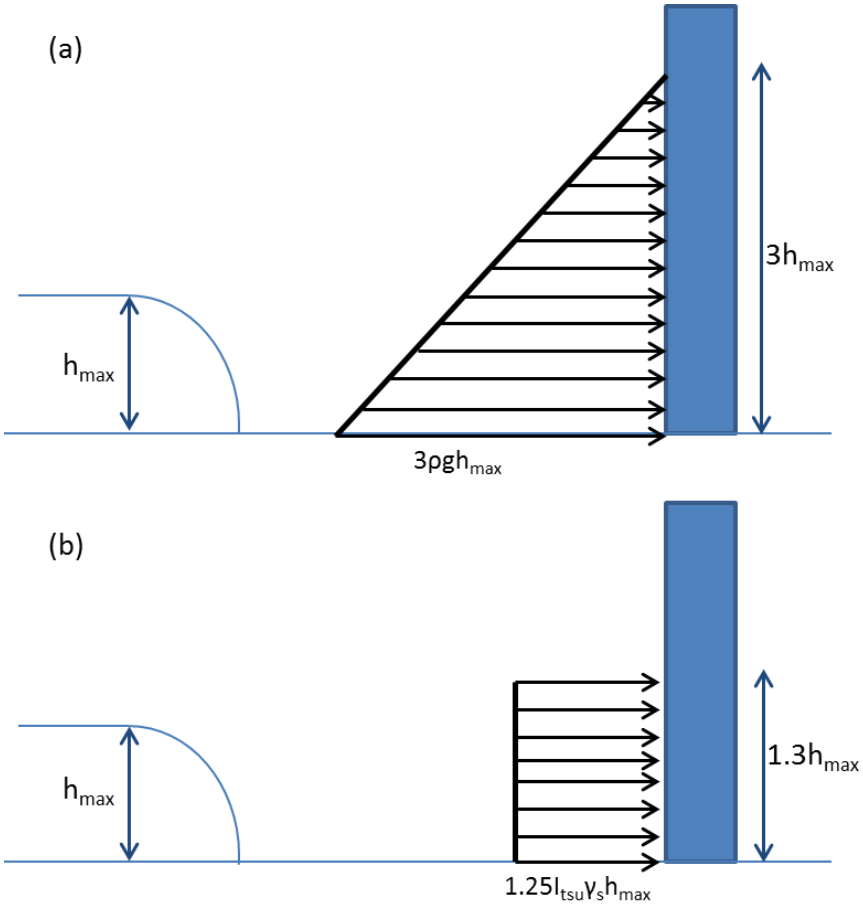

Figure 1: Design tsunami pressure distribution, as recommended by (a) JCO (2005), and (b) ASCE 7 (2015).

Prior to 2011, no design guidelines existed in the United States for estimating tsunami-induced pressures on coastal structures. This circumstance was partially because the United States has experienced fewer damaging tsunamis than other regions in the Pacific Ocean; the most destructive tsunami affecting the West Coast of North America was the 1964 Great Alaska Earthquake Tsunami, which caused damage and loss of life in Alaska, California, Oregon, and British Columbia (Parsons, et al., 2014). However, many areas of the United States remain vulnerable to damage by earthquake-generated tsunamis. Therefore, in early 2011, the ASCE developed a subcommittee to develop the first U.S. standard for use by coastal engineers to design coastal structures with increased resilience to tsunami damage. These standards will be published in ASCE 7-16 as a new chapter (ASCE, 2014) and have been developed for the Pacific Coast of the United States. The guidelines include tsunami hazard maps for Alaska, the Pacific Coast, and Hawaii, and the chapter provides procedures for estimating tsunami inundation, runup, flow characteristics, and hydrostatic and hydrodynamic loads (ASCE, 2015). Equation 6.10.1-1 (ASCE, 2015) presents the following equation to estimate the simplified equivalent uniform lateral static pressure (p_{max}), which represents the combination of the unbalanced lateral hydrostatic and hydrodynamic loads caused by a tsunami:

$$p_{max} = 1.25 I_{tsu} \gamma_s h_{max} \quad (3),$$

In Equation (3), I_{tsu}=1.0 or 1.25 based on the Importance Factor of the structure and γ_s is the minimum fluid weight density for hydrostatic loads, equal to 1.1 times the specific weight of seawater. Substituting conservative coefficients for I_{tsu}, and γ_s, Equation (3) may be reformulated to resemble Equation (1):

$$p_{max} = 1.72 \rho g h_{max} \quad (4).$$

Comparison of Equations (1) and (4) imply that the ASCE recommended pressure is less conservative than the JCO equation. Note, also, that ASCE recommends a different pressure distribution when estimating the tsunami-induced force on

a structure, applying p_{max} uniformly over 1.3 times the inundation depth in the direction of flow (Figure 1b).

INSTRUMENTATION AND EXPERIMENTAL CONDITIONS

HyTOFU measures 45 m long by 4 m wide by 2 m deep. It is capable of three types of wave generation mechanisms: a mechanical piston capable of producing a solitary wave with height up to 1 m, a 70 Kw pump that can produce constant flow rates between 0 and 0.8 m^3/s, and a constant volume water storage tank that can be dropped from a distance above the water surface to induce a shock wave. A profile view of the flume may be seen in Figure 2; in this experiment, a constant flow rate was generated for 60 seconds before the mechanical paddle was used to create a wave that propagated 14.05 m across a flat bathymetry with initial water depth h_0=0.700 m, up a 7.95 m long slope with θ=0.10, and across a flat beach to the end of the flume.

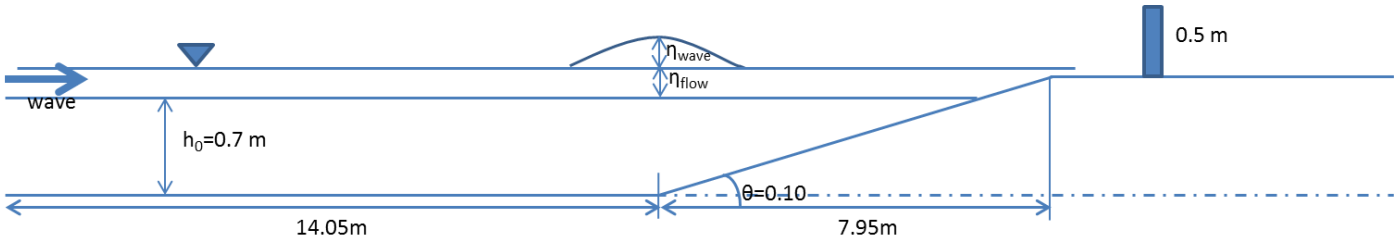

Figure 2: Profile schematic of hydraulic flume. Wave characteristics were measured near the base of the slope (x_{wg2}=14.50 m). Onshore water surface elevations were compared with and without an obstacle present.

Experiments were conducted using a 1:20 length scale and Froude Number similitude: target offshore water perturbations between 0.40 m and 0.48m were specified to represent waves with amplitudes between 8 m and 9.6 m, and the dimensions of the structural element (0.4 m wide x 0.4 m long x 0.5 m tall) corresponded with those of a narrow Japanese house with base dimensions 8 m x 8 m. The water surface elevation was recorded using wire resistance wave gauges. Mechanical and pumping inputs were chosen to create waves with similar offshore total water surface perturbations ($\eta_{wave}+\eta_{flow}$) while varying the ratio of the mechanically-generated wave height (η_{wave}) to the total water perturbation produced by the combination of pumping flow (η_{flow}) and mechanical soliton (η_{wave}). Wave characteristics were defined at wave gauge 2 (WG2), positioned near the base of the slope, x_{WG2}=14.50 m. Table 1 shows the seven combinations of mechanically-generated waves and pump-generated flow rates used for experimental measurements, as well as the ensemble average and standard deviation of the total water surface perturbation for all trials. Each of the seven test conditions listed in Table 1 was generated twice for each experimental configuration to check the repeatability of wave characteristics; as seen in Table 1, waves with the same inputs were nearly identical for all configurations. Wave combinations were generated for three configurations: one configuration with no onshore obstacles and two configurations with obstacles positioned at locations shown in Figure 3, either (a), 2.39 m, or (b), 1.59 m from shore. We compared the water surface elevation time series with and without obstacles at wave gauges located directly in front of the structure, for configuration (a), x_{WG11}=2.3 m, and for configuration (b), x_{WG9}=1.3 m to evaluate the effects of adding a macro-roughness element on variation in the water surface profile.

Table 1: Experimental combinations of mechanically-generated wave and pump flow inputs and average water surface perturbation above h=0.700 m at horizontal position x=14.50 m for each trial. Tests produced waves of varying characteristics but similar total water surface perturbations at x=14.50 m.

Test	Mechanical Input (m)	Pump Input (m^3/s)	$(\overline{\eta_{wave}+\eta_{flow}})$ (cm) x=14.50 m	Standard deviation (cm)
1	0	0.80	40.85	0.10
2	0.10	0.60	41.29	0.14
3	0.15	0.40	39.80	0.27
4	0.20	0.30	40.26	0.12
5	0.25	0.20	39.61	0.16
6	0.35	0.10	41.94	0.12
7	0.40	0.10	47.789	0.16

In addition to measuring the water surface elevation, 50 kPa pressure gauges were mounted on the front, lateral, and rear sides of the structural element to measure the wave impact pressure and following quasi-hydrostatic pressure. On the front side of the structural element, nine pressure gauges were positioned in three rows of three at elevations 0.01 m, 0.05 m, and

0.15 m. On the lateral and back sides, seven pressure gauges were positioned in two rows of three at elevations 0.01 m and 0.05 m with one gauge located at elevation 0.15 m along the centerline of the face of the structure. Pressure gauge data was recorded using a frequency of 200 Hz to record the short-duration impulse spike felt by the obstacle upon impact with breaking waves. Data was checked for contamination by local utility frequencies using a band pass filter. Cleaned and raw pressure data were compared, and peak pressure recordings differed by less than 5%. The maximum recorded pressure for all experiments was by a gauge mounted on the front face of the specimen.

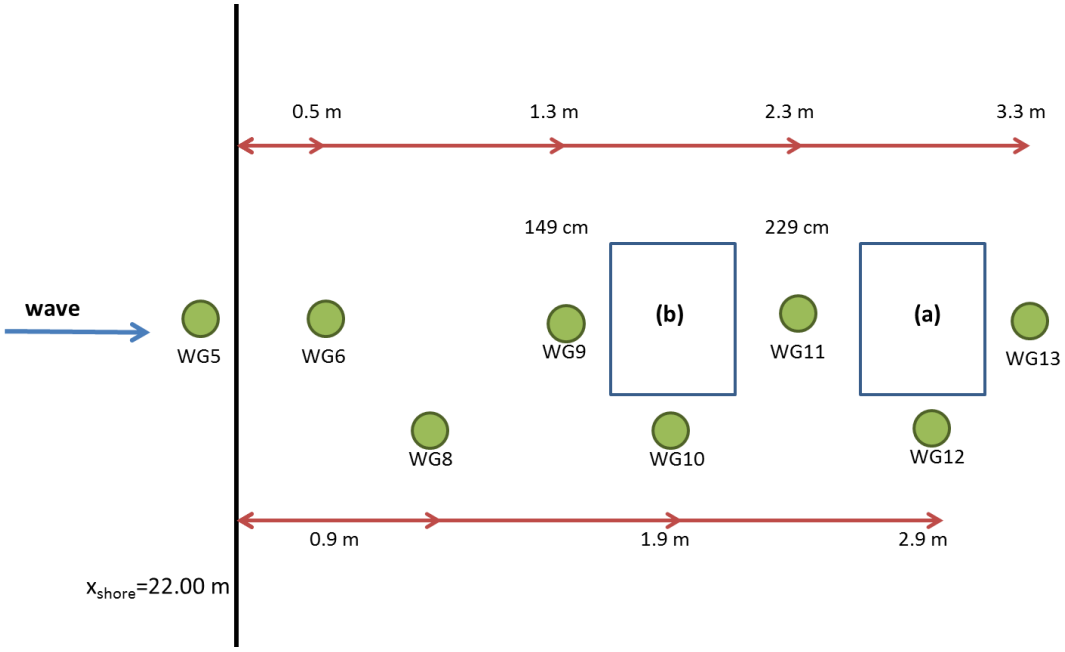

Figure 3: Schematic of experiment. Water surface elevations 2.3 m and 1.3 m from shoreline with no obstacles present were compared with water surface elevations when an obstacle was positioned at either (a) or (b), behind the wave gauges.

RESULTS AND DISCUSSION

Figure 4 shows a comparison of the water surface elevation time series with and without macro-roughness effects for configurations (a) and (b) for the wave generated using inputs for Trial 7 in Table 1. The control, bare-earth time series in Figure 4 indicates that the wave propagated past both wave gauges positioned 2.3 m and 1.3 m from shore with a very low water surface elevation η; visual observation and video analysis of the trial confirmed that the wave passed these gauges as a turbulent bore with a high propagation speed. As seen in Figure 4, adding a structure significantly changed the water surface profile when the wave propagated past the location of interest. When the wave impacted the obstacle, the interaction of the wave with the structure created a large vertical jet that was nearly five times the height of the water surface elevation with no obstacle present for the wave gauge positioned 1.3 m from shore and over five times that for the wave gauge positioned 2.3 m from shore. Configurations (a) and (b) showed similar splash effects; however, the water series comparison when the obstacle was positioned further inland (Figure 4a) recorded a larger splash than that of the obstacle positioned 1.59 m from shore (Figure 4b) despite having a lower peak water surface elevation when the wave propagated across the no-obstacle topography. Therefore, the difference between numerically-predicted water surface elevations by models which remove macro-roughness elements and true water surface profiles may increase moving inland while waves still contain a great amount of energy. Moving further inland, however, waves are expected to dissipate, and these weaker waves are expected to create smaller splash effects when they come in contact with macro-roughness elements. Therefore, after a certain distance inland, error in numerical simulations should decrease with increasing distance from shore.

In Table 1, Trial 7 was generated by the largest mechanical wave input (0.40 m target wave height) and the smallest pumping flow input (0.10 m^3/s). Other trials considered waves with increased flow rates and decreased mechanical soliton inputs. To parameterize these varying wave characteristics, we defined the offshore solitary wave fraction as the ratio of the mechanically-generated wave perturbation η_{wave} to the total water surface perturbation above the stillwater depth caused by both the constant flow and the mechanical wave ($\eta_{wave}+\eta_{flow}$):

$$\eta^* = \frac{\eta_{wave}}{\eta_{wave} + \eta_{flow}} \quad (5).$$

As the wave profile approaches that of a solitary wave, with no constant-flow water level increase, η* approaches 1. Likewise, for pure pumping conditions in which the water level steadily increases but no mechanical wave is generated, both η_{wave} and η* equal 0. Such a condition can be thought of as similar to the water level rise associated with a storm surge generated by a hurricane.

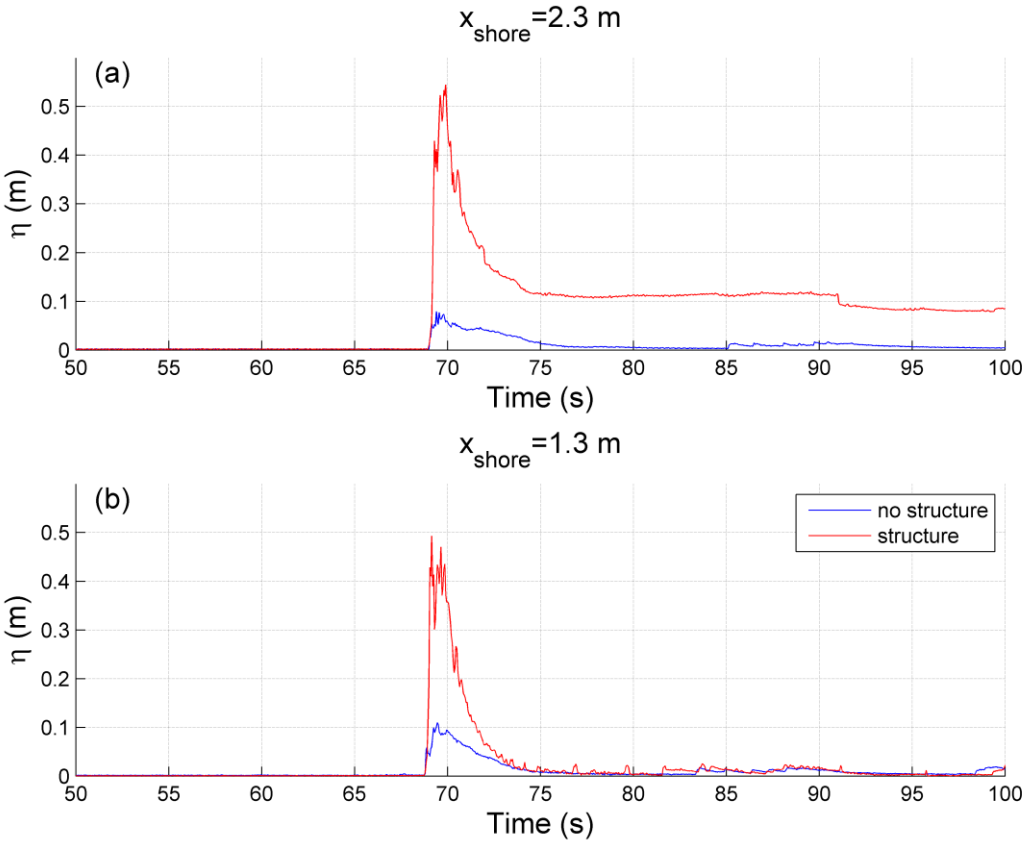

Figure 4: Macro-roughness-induced wave reflection and amplification. Water surface elevation time series for Trial 7 (0.4 m mechanical wave generated after one minute of pumping flow at 0.1 m^3/s) at (a) x_{WG11}=2.3 m (b) x_{WG9}=1.3 m from shore. Blue line: no onshore structure; and red line: obstacle positioned behind the respective WG.

In experiments, waves with large pumping flow inputs corresponded to those with small solitary wave fractions (η*<0.5); these waves did not break on the obstacle. Because splashing is associated with turbulent effects caused by a wave breaking on an obstacle, we expected the maximum difference between water surface elevations with and without a structure to occur for larger values of η*. This hypothesis was confirmed by comparing the maximum water surface elevation including splash ($\eta_{obstacle}$) to that recorded when no structure was behind the wave gauge ($\eta_{no\ obstacle}$). The ratio $\eta_{obstacle}/\eta_{no\ obstacle}$ was plotted against η* for Trials 1-7 of Table 1 for both configurations (a) and (b) in Figure 5. For both setback distances, increasing values of η* corresponded with larger water surface amplification ratios. As η* approached 1, $\eta_{obstacle}/\eta_{no\ obstacle}$ increases rapidly. Note that increasing the obstacle setback distance from 1.59 m to 2.39 m increased the water surface amplification ratio for Trials 6 and 7. However, positioning the obstacle a large enough distance from shore so that waves can dissipate is expected to reduce the water surface amplification caused by wave-structure interaction.

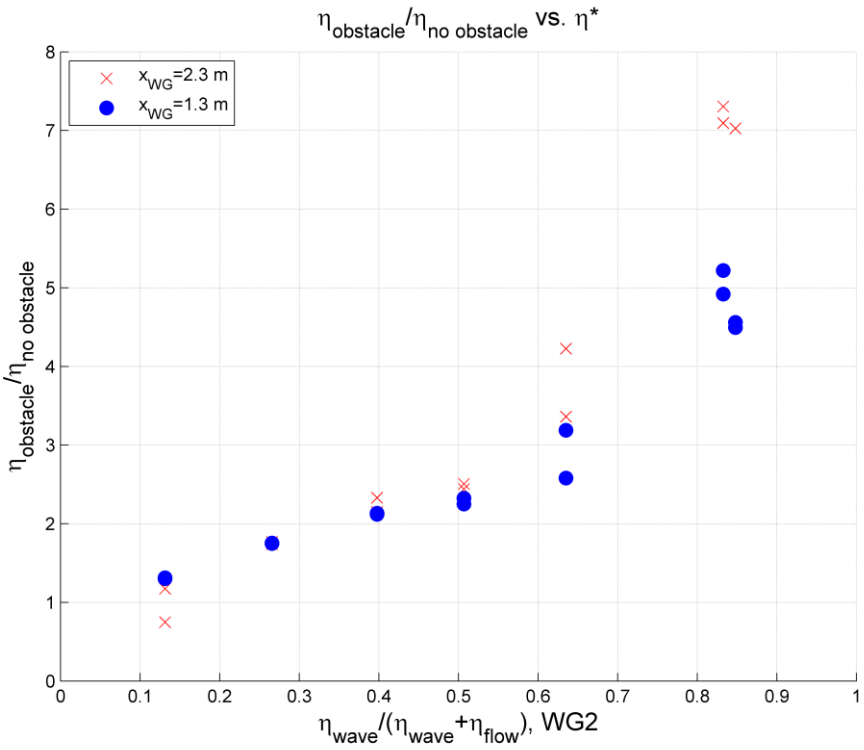

Figure 5: Ratio of maximum water surface elevation with an obstacle ($\eta_{obstacle}$) to that measured with no structures ($\eta_{no\ obstacle}$). $\eta_{obstacle}/\eta_{no\ obstacle}$ increased with the solitary wave fraction for both setback distances 2.3 m (red exes), and 1.3 m (blue circles).

As discussed above, many design equations for estimating the maximum tsunami-induced pressure use the water surface elevation in front of the structure without considering wave-structure interaction. We evaluated Equation (1) and Equation (4) using the water surface elevation recorded in the bare-earth trial, and compared these estimated values with peak pressures measured during experiments. Figure 6 shows the pressures predicted by design equations plotted against the measured peak pressures for both setback configurations (a) and (b). As seen in the figure, disregarding water surface amplification caused by wave-structure interaction and using no-obstacle water surface elevations in prediction agreed reasonably well for low pressures, which were associated with nonbreaking wave conditions. However, after wave breaking, design equations using h_{max} without considering wave amplification due to macro-roughness generally underestimated measured peak pressures. Equations (1) and (4) were reevaluated with modified h_{max} inputs, taking h_{max} as the maximum water surface elevation recorded when the structure was positioned in the flume. As shown in Figure 6, using these modified inputs in the equations produced better agreement between estimated tsunami pressures and experimentally measured peak pressures caused by breaking waves. In particular, the equation suggested by the JCO (2005) agreed well with even the largest pressure measurements for both configurations, and it produced conservative estimations of peak pressures for nonbreaking wave cases. The equation provided by the ASCE (2015) agreed well for low and intermediate pressures, but still underestimated the maximum peak pressures recorded by the structural element. Better understanding of the environmental conditions occurring at a structure and the processes associated wave impact may provide a more reliable estimation of expected peak pressures.

Note that both the ASCE and Asakura design equations provide conservative pressure distributions for estimating the total force associated with a tsunami wave impacting a coastal structure. Therefore, the overall force predicted by design equations may be conservative, even using the recommended bare-earth input for h_{max}. Additionally, Cooker and Peregrine (1995) noted that laboratory experiments may record pressures that are significantly larger than those recorded in the field. Although there remains some debate as to whether the large pressure peaks associated with wave impact translate to a force on large inertia structures and need to be included in design (Bradner, 2009), these large impulsive pressures should not be neglected in the design of coastal residences, particularly when considering small inertia structures or localized damage to house components.

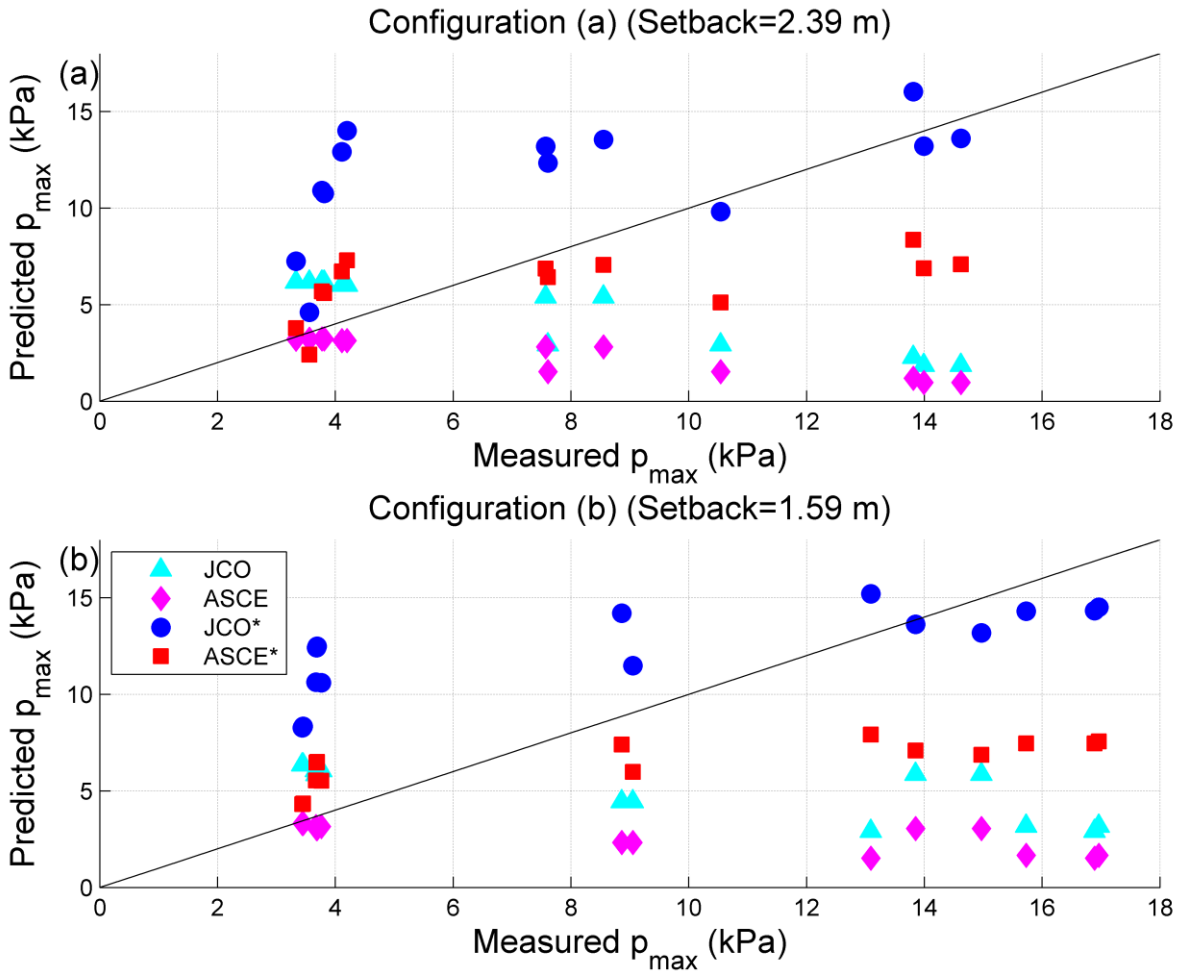

Figure 6: Predicted vs. measured peak pressure for configurations (a), obstacle positioned 2.39 m from shore, and (b), obstacle positioned 1.59 m from shore. Cyan triangles: JCO (2005) equation, $h_{max}=h_{no\ obstacle}$; magenta diamonds: ASCE (2015) equation, $h_{max}=h_{no\ obstacle}$; blue circles: JCO (2005) equation, $h_{max}=h_{obstacle}$, red squares: ASCE (2015) equation, $h_{max}=h_{obstacle}$.

CONCLUSIONS

Experiments conducted at Kyoto University's Hybrid Tsunami Open Flume in Ujigawa generated a benchmark data set that showed that the addition of urban macro-roughness elements significantly affected wave propagation and transformation onshore. The water surface elevations of waves propagating across a bare beach was significantly different than those measured when obstacles were positioned onshore, especially for waves that broke before the obstacle and travelled across the beach as high velocity, turbulent bores. The effect of macro-roughness elements on a wave's profile may therefore cause errors in numerical models that calculate water surface elevations and velocities using the post-storm, bare-earth topography of a region. For breaking waves, this error is expected to increase up to a certain distance inland, at which point the largest energy transfer occurs when a wave interacts with a structure, thus maximizing the amplification of the water surface. As waves lose energy propagating further inland, error in numerical models should likewise decrease.

Water surface elevations measured with and without onshore structures were applied to design equations recommended by both the ASCE (2015) and JCO (2005). Using bare-earth water surface elevations in design equations yielded pressures that agreed with measured peak pressures for nonbreaking waves. However, these bare-earth inputs for h_{max} significantly underestimated measured peak pressures for breaking waves. In contrast, using modified water surface elevations that included the effects of wave-structure interaction provided much closer agreement between predicted and measured pressures for breaking wave trials. In particular, using modified h_{max} values in Equation (1) produced good agreement between estimated and measured peak pressures as η^* approached one, and the equation resulted in conservative estimates for trials with smaller solitary wave fractions.

In practice, a coastal engineer must account for case-specific parameters associated with local bathymetry, community layout, and offshore wave characteristics. Therefore, the pressures measured here may not directly apply to structural design criteria. In addition, due to the short duration of these very large impact pressures, such conservative design should be applied to structures of significant community importance, and more research is required to fully understand the effects of impulsive wave loads on coastal structures. However, coastal structures must be designed to resist the hydrodynamic loads generated by tsunamis, including wave impacts on structural components, debris impact, and other uncertainties. Engineers, city planners, and homeowners must work together to understand the full effects of macro-roughness elements on wave propagation so that we may find cost-effective, innovative design techniques that prepare our coastal communities to robustly withstand future tsunami events.

ACKNOWLEDGEMENT

The authors wish to thank all those who assisted with experiments and analysis. This material is based upon work supported by the National Science Foundation (NSF) Graduate Research Fellowship under Grant No. 2013115239. Any opinions, findings, and conclusions or recommendations expressed in this material are those of the authors and do not necessarily reflect the views of the National Science Foundation. Additional funding was provided by the Japan Society for the Promotion of Science (JSPS) in collaboration with the NSF Graduate Research Opportunities Worldwide (GROW) Program (GR14004), and the Disaster Prevention Research Institute (DPRI).

REFERENCES

ASCE. (2014). "New chapter on tsunami design in ASCE 7-16." *ASCE.* ASCE, 23 January 2014. Web. 20 October 2015. http://www.asce.org/structural-engineering/news/20140123-new-chapter-on-tsunami-design-in-asce-7-16/

ASCE. (2015). "Minimum design loads for buildings and other structures: Chapter 6 Tsunami Loads and Effects." *ASCE/SCI 7-16*, New York.

Achmed F., Shigihara,Y., Fujima, K., Mizutani, N. (2009). "Experimental Study on tsunami forces: Estimation of tsunami force acting on structures related to runup distance, scakle of building and pressure distribution." *Proceedings of the 5th International Conference on Asian and Pacific Coasts.* 13-18 October 2009. Singapore.

Asakura, R., Iwase, K., and Iketani, T. (2000). "Proceedings of the Coastal Engineering of JSCE" **(47)** 911-915.

Bagnold, R.A. (1939). "Interim report on wave pressure research." *Journal of the Institution of Civil Engineers.* **12,** 202-226.

Bradner, C., Schumacher, T., Cox, D., Higgins, C., 2009. Large scale laboratory measurements of wave forces on highway bridge superstructures. Proceedings of the 31st International Conference, Hamburg, Germany. 3554-3566.

Bullock, G.N., Obhrai, C., Peregrine, D.H., and Bredmose, H. (2007). "Violent breaking wave impacts. Part 1: Results from large-scale regular wave tests on vertical and sloping walls." *Coastal Engineering.* **54 (2007).** 602-617.

Chen, E.S., and Melville, W.K., (1988). "Deep-waetr plunging wave pressures on a vertical plane wall." *Proc. R. Soc. London. A.* **417,** 95-131.

Cooker, M.J. and Peregrine, D.H. (1995). "Pressrue impulse theory for liquid impact problems." *J. Fluid Mech.* **297,** 193-214.

Dalrymple, R.A. and Kriebel, D.L. (2005). "Lessons in Engineering from the Tsunami in Thailand." *Bridge*, **35** (2)**.** 4-13.

Fujima, K., Achmad, F., Shigihara, Y.,Mizutani, N., 2009. "Estimation of tsunami force acting on rectangular structures*." Journal of Disaster Research*, 4 (6), 404e409.

Goseberg N., Wurpts A., Schlurmann T. 2013. "Laboratory-scale generation of tsunami and long waves." *Coastal Engineering*, 79:57 - 74.

Grilli, S., O'Reilly, C., Harris, J., Bakhsh, T.T., Tehranirad, B., Banihashemi, S., Kirby, J., Baxter, C., Eggeling, T., Ma, G., Shi, F., (2015). "Modeling of SMF tsunami hazard along the upper US East Coast: detailed impact around Ocean City, MD." *Nat Hazards*, **76**, 705-746.

Hsiao, S., and Lin, T., (2010). "Tsunami-like solitary waves impinging and overtopping an impermeable seawall: Experiment and RANS modeling." *Coastal Engineering,* **57**,1-18.

JCO/Task Committee under the Japanese Cabinet Office (2005). "Design Guidelines for Tsunami Shelters" (in Japanese), http://www.bousai.go.jp/oshirase/h17/ tsunami_s iryo 2.pdf

Kawai, H., Satoh, M., Kawaguchi, K., Seki, K. (2012). "Recent tsunamis observed by GPS buoys off the Pacific coast of Japan." *Coastal Engineering Proceedings,* **33,** 1-15.

Koshimura, S., Oie, T., Yanagisawa, H., and Imamura, F.. (2009). "Developing fragility functions for tsunami damage estimation using numerical model and post-tsunami data from Banda Aceh, Indonesia." *Coastal Engineering Journal,* **51**(3). 243-273.

Leone, F., Lavigne, F., Paris, R., Denain, J.C., and Vinet, F. (2011). "A spatial analysis of the December 26th, 2004 tsunami-induced damages: Lessons learned for a better risk assessment integrating buildings vulnerability." *Applied Geography,* **31**(1), 363-375.

Lynett, P., Wu, T., Liu, P. (2002). "Modeling wave runup with depth-integrated equations." *Coastal Engineering,* **46,** 89-107.

Ma, G., Shi, F., Kirby, J.T. (2012). "Shock-capturing non-hydrostatic model for fully dispersive surface wave processes." *Ocean Modelling,* **43-44,** 22-35.

Mas, E., Koshimura, S., Suppasri, A., Matsouka, M., Matsuyama, M., Yoshii, T., Jimenez, C., Yamazaki, F., Imamura, F. (2012).

"Developing Tsunami fragility curves using remote sensing and survey data of the 2010 Chilean Tsunami in Dichato." *Nat Hazards*, **12,** 2689-2697.

Mimura, N., Yasuhara, K., Kawagoe, S., Yokoki, H., and Kazama, S. (2011). "Damage from the Great East Japan Earthquake and Tsunami-A quick report." *Mitigation and Adaptation Strategies for Global Change.* **(16)**7, 803-818.

Mori, N., Takahashi, T, Yasuda, T., YAnagisawa, H. (2011). "Survey of 2011 Tohoku earthquake tsunami inundation and run-up." *Geophysical research letters*, **38**(7), L00G14.

Nakano, Y. (2008). "Design load evaluation for tsunami shelters based on damage observations after Indian Ocean Tsunami disaster due to the 2004 Sumatra Earthquake." *The 14th World Conference on Earthquake Enginering*, 12-17 October, 2008. Beijing, China.

Papadopoulous, G.A., Caputo, R., McAdoo, B., Pavlides, S., Karasthis, V., Fokaefs, A., Orfanogiannaki, K., and Valkaniotis, S. (2006). "The large tsunami of 26 December 2004: Field observations and eyewitnesses accounts from Sri Lanka, Maldives Is. and Thailand." *Earth Planets and Space*, **58**(2). 233-241.

Parsons, T., Geist, E., Ryan, H., Lee, H., Haeussler, P., Lynett, P., Hart, P., Sliter, R., Roland, E. (2014). "Source and progression of a submarine landslide and tsunami: The 1964 Great Alaska earthquake at Valdez." *J. of Geophysical Research: Solid Earth*, **119,** 8502-8516.

Peregrine, D.H., (2003). "Water wave impacts on walls." *Annual Rev. Fluid Mech.* **35**, 23-43.

Petukhin, A., Yoshida, K., and Miyakoshi, K. (2012). "Tsunami simulation for the 2011 Great Tohoku earthquake (Mw9.0), Japan, using seismic inversion source model and fully nonlinear tsunami model." *Fifteenth world conference on earthquake engineering.* Lisboa.

Suppasri, A., Koshimura, S., Imamura, F. (2011). "Developing tsunami fragility curves based on the satellite remote sensing and the numerical modeling of the 2004 Indian Ocean tsunami in Thailand." *Nat Hazards Earth Syst. Sci.,* **11,** 173-189.

Suppasri, A., Mas, E., Charvet, I., Gunasekera, R., Imai, K., Fukutani, Y., Abe, Y., Imamura, F. (2013). "Building damage characteristics based on surveyed data and fragility curves of the 2011 Great East Japan tsunami." *Nat Hazards*, **66**, 319-341.

Reese, S., Bradley, B.A., Bind, J., Smart, G., Power, W., Sturman, J. (2011). "Empirical building fragilities from observed damage in the 2009 South Pacific tsunami." *Earth-Science Reviews.* **107**(1-2), 156-173.

Tsuji, Y., Namegaya, Y., Matsumoto, H., Iwasaki, S.I., Kanuba, W., Sriwachai, M., and Meesuk, V. (2011). "The 2004 Indian tsunami in Thailand: Surveyed runup heights and tide gauge records." *Earth Planets and Space*, **58**(2). 223-232.

Udo, K., Sugawara, D., Tanaka, H., Imai, K., and Mano, A. (2012). "Impact of the 2011 Tohoku Earthquake and Tsunami on Beach Morphology along the Northern Sendai Coast." *Coastal Engineering Journal*, **54**(1). 1250009.

Westerink, J.J., Luettich, R.A., Feyen, J.C., Atkinson, J.H., Dawson, C., Roberts, H., Powell, M.D., Dunion, J.P., Kubatko, E.J., Pourtaheri, H. (2008). "A Basin- To Channel-Scale Unstructured Grid Hurricane Storm Surge Model Applied To Southern Louisiana." *Monthly Weather Review*, **136**(3)**.** 833-864.

Yeh, H. (2009). "Tsunami impacts on coastlines." *The Sea: Tsunamis.* Ed. Eddie N. Bernard, Allan R. Robinson. Cambridge: Harvard University Press, 2009. 333-370.

Zaré, M. and Afrouz, S.G. (2012). "Crisis Management of Tohoku; Japan Earthquake and Tsunami, 11 March 2011." *Iranian Journal of Public Health.* **41**(6), 12-20.

Zhang Yao, Kennedy, A.B., Aaron S. Donahue, Westerink, J.J., Panda, N., Dawson, C.(2014a)."Rotational Surf Zone Modeling for O(mu4) Boussinesq-Green-Naghdi Systems." *Ocean Modeling*, **79,** 43-53.